Inorganic Chemistry

Article

pubs.acs.org/IC

# Preparation, Structural Characterization, and Ion-Exchange Properties of Two New Zeolite-like 3D Frameworks Constructed by ε-Keggin-Type Polyoxometalates with Binding Metal Ions, $H_{11.4}[ZnMo_{12}O_{40}Zn_2]^{1.5-}$ and $H_{7.5}[Mn_{0.2}Mo_{12}O_{40}Mn_2]^{2.1-}$

Zhenxin Zhang,[†] Masahiro Sadakane,*[,‡,§] Toru Murayama,[†] Norihito Sakaguchi,[∥] and Wataru Ueda*[,†]

[†]Catalysis Research Center, Hokkaido University, N-21, W-10 Kita-ku, Sapporo 001-0021, Japan

[‡]Department of Applied Chemistry, Graduate School of Engineering, Hiroshima University, 1-4-1 Kagamiyama, Higashi, Hiroshima 739-8527, Japan

[§]PRESTO, JST, 4-1-8 Honcho, Kawaguchi, Saitama 332-0012, Japan

[∥]High Voltage Electron Microscope Laboratory, Center for Advanced Research of Energy Conversion Materials, Hokkaido University, N-13, W-8, Sapporo 060-8626, Japan

Supporting Information

**ABSTRACT:** Two new ε-Keggin-type polyoxometalate-based 3D frameworks, $Na_{1.5}H_{11.4}[\varepsilon\text{-}Zn^{II}Mo^{V}_{10.9}Mo^{VI}_{1.1}O_{40}\{Zn^{II}\}_2]$ and $(NH_4)_{2.1}H_{7.5}[\varepsilon\text{-}Mn^{II}_{0.2}Mo^{V}_{6}Mo^{VI}_{6}O_{40}\{Mn^{II}\}_2]$, are prepared, and their structures are determined by powder X-ray diffraction, Fourier transform infrared, Raman spectroscopy, and elemental analysis. ε-Keggin-type polyoxomolybdate units, $[\varepsilon\text{-}ZnMo_{12}O_{40}]$ and $[\varepsilon\text{-}Mn_{0.2}Mo_{12}O_{40}]$, are linked with $Zn^{2+}$ and $Mn^{2+}$, respectively, in a tetrahedral fashion to form 3D frameworks. They show zeolite-like ion-exchange properties and redox properties. The ε-Keggin-based 3D framework shows high chemical composition diversity and can incorporate different elements in the framework.

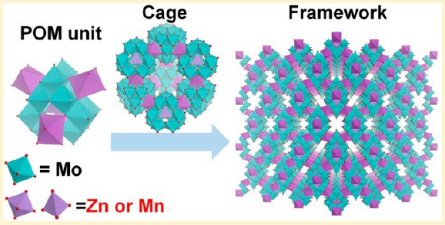


## INTRODUCTION

Polyoxometalates (POMs) are anionic metal oxide clusters comprised of mainly early transition metals such as tungsten, molybdenum, niobium, and vanadium.[1−3] POMs have attracted much attention because they are applicable to functional materials, such as catalysts and electrode, optical, and magnetic materials. Furthermore, their molecular properties, such as multielectron-transfer, strong acidic, and magnetic properties, are tunable by changing their structures and incorporating metal components in the structures.

POMs are also known to be well-defined building units for the construction of nanostructured materials and well-ordered crystalline materials, such as polyoxometalate−organic frameworks (POMOFs),[4−10] macrocations−POM materials,[11−18] and complex metal oxides.[19−21] These materials have been prepared by the assembly of POMs with other structural building blocks. The resulting materials exhibit interesting properties and have various applications, such as adsorption,[11,12,22,23] separation,[11,12] catalysis,[16,20,24−27] ion exchange,[28] and electrocatalysis.[6] The most popular POM building unit is the α isomer of a Keggin-type POM.

In the case of POMOF materials, the ε isomer of a Keggin-type POM composed of one central $XO_4$ tetrahedron and 12 metal−oxygen octahedra with $T_d$ symmetry is of great interest. Four hexagonal faces of the ε-Keggin POM are bound to metal ions (Figure 1), and linking of these four metal ions by a bidentate organic ligand results in the formation of a 3D-ordered framework of POM and an organic moiety.[4,6,7] Recently, we have reported the first all-inorganic 3D framework composed of ε-Keggin POM, $[\varepsilon\text{-}VMo_{9.4}V_{2.6}O_{40}]$, with a bismuth linker (denoted as Mo−V−Bi oxide). A total of 10 $[\varepsilon\text{-}VMo_{9.4}V_{2.6}O_{40}]$ units surround a cage that is connected by channels, forming a zigzag 3D pore system.[29] Compared with POMOFs, the Mo−V−Bi oxide is thermally more stable so that water and ammonium cations presented in the pores can be removed by thermal treatment, and the opened pores are analyzable by the $N_2$ adsorption−desorption technique. Furthermore, ammonium cations are exchangeable with other cations.

One of the important properties of POMs is diversity of the elements in the structures, and it is desirable for many kinds of elements to be able to be incorporated into the structures of ε-Keggin POM-based 3D frameworks and their properties, such as stability, ion-exchange property, acidity, and redox, magnetic, and pore properties, to be easily tuned.

Here, we describe the synthesis and structural characterization of two new members of all-inorganic ε-Keggin POM-based 3D frameworks, ε-Keggin polyoxomolybdates with metal ions ($Zn^{II}$ and $Mn^{II}$), $Na_{1.5}H_{11.4}[\varepsilon\text{-}Zn^{II}Mo^{V}_{10.9}Mo^{VI}_{1.1}O_{40}\{Zn^{II}\}_2]$ and $(NH_4)_{2.1}H_{7.5}[\varepsilon\text{-}Mn^{II}_{0.2}Mo^{V}_{6}Mo^{VI}_{6}O_{40}\{Mn^{II}\}_2]$, denoted as Mo−Zn oxide and

**Received:** March 19, 2014
**Published:** July 9, 2014

   dx.doi.org/10.1021/ic500630h | Inorg. Chem. 2014, 53, 7309−7318

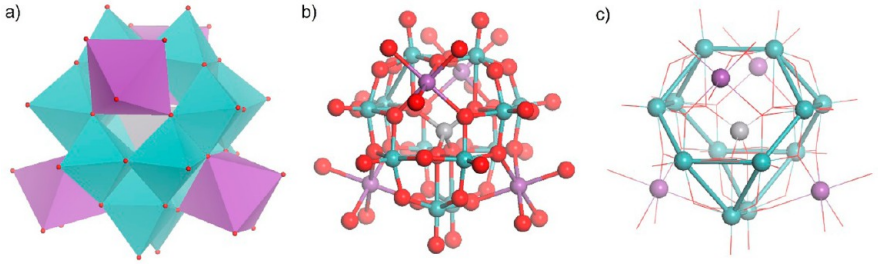


**Figure 1.** (a) Polyhedral representation, (b) ball–stick representation, and (c) metal skeleton representation of $\varepsilon$-Keggin-type POM with four capping metal ions. Central metal site: gray. Surrounding metal site: blue. Linking metal: purple. Oxygen: red.

Mo–Mn oxide, respectively. Structures of the materials are determined by powder X-ray diffraction (XRD), Fourier transform infrared (FT-IR), and elemental analysis. The thermal stability of the materials is investigated, and it is found that the existing guest molecules can be mostly removed by heat treatment. The materials are found to have selective ion-exchange properties that are similar to those of zeolites.

## EXPERIMENTAL SECTION

**Materials.** All chemicals were of reagent grade and were used as supplied, and house-made distilled water was used throughout. Mo–V–Bi oxide was prepared according to our paper.[29]

**Synthesis of Mo–Zn Oxide.** $Na_2MoO_4{\cdot}2H_2O$ (2.823 g, 11.7 mmol based on Mo) was dissolved in 40 mL of distilled water. Metal Mo (0.2 g, 2.1 mmol) and $ZnCl_2$ (0.453 g, 3.3 mmol) were added to the mixture sequentially, followed by adjustment of the pH to 4.8 with 1 M $H_2SO_4$. The mixture was introduced into a 50 mL Teflon liner of a stainless-steel autoclave. The autoclave was placed in an oven heated at 448 K for 24 h. After the autoclave had been cooled to room temperature, the mixture was placed in a 100 mL beaker. For solid recovery, 60 mL of water was added to the beaker, and the beaker was kept at room temperature for 5 min. Then the upper 50% part of the suspension was collected by filtration. The recovery process was repeated three times. The resulting solid was washed with 10 mL of water three times and dried at 353 K overnight. Then 0.28 g of Mo–Zn oxide (yield: 14% based on Mo) was obtained. Elem anal. Calcd for $Na_{1.5}Zn_3Mo_{12}O_{45}H_{21.4}$: Zn, 9.24; Mo, 54.22; Na, 1.62; H, 1.02. Found: Zn, 9.63; Mo, 54.14; Na, 1.54; H, 1.18.

**Synthesis of Mo–Mn Oxide.** $(NH_4)_6Mo_7O_{24}{\cdot}4H_2O$ (2.060 g, 11.7 mmol based on Mo) was dissolved in 40 mL of distilled water. Metal Mo (0.2 g, 2.1 mmol) and MnO (0.235 g, 3.3 mmol) were added to the mixture sequentially (pH of 5.1). The mixture was introduced into a 50 mL Teflon liner of a stainless-steel autoclave. The autoclave was placed in an oven heated at 448 K for 24 h. After the autoclave had been cooled to room temperature, the mixture was placed in a 100 mL beaker. For solid recovery, 60 mL of water was added to the beaker, and the beaker was kept at room temperature for 5 min. Then the upper 50% part of the suspension was collected by filtration. The recovery process was repeated three times. The resulting solid was washed with 10 mL of water three times and dried at 353 K overnight. Then 0.32 g of Mo–Mn oxide (yield: 16% based on Mo) was obtained. Elem anal. Calcd for $N_{2.1}Mn_{2.2}Mo_{12}O_{44}H_{23.9}$: Mn, 5.95; Mo, 56.72; N, 1.45; H, 1.19. Found: Mn, 5.91; Mo, 56.45; N, 1.62; H, 1.23.

**Ion Exchange.** As-synthesized material (Mo–Zn oxide or Mo–Mn oxide, 0.3 g) was dispersed in 15 mL of water containing 0.61 mmol each of LiCl, NaCl, $NH_4Cl$, KCl, RbCl, CsCl, $BeSO_4$, $MgCl_2$, $CaCl_2$, $SrCl_2$, and $BaCl_2$. The mixture was stirred at 353 K for 6 h. The resulting solid (M–Mo–Zn oxide or M–Mo–Mn oxide, where M = Li, Na, $NH_4$, K, Rb, Cs, Be, Mg, Ca, Sr, and Ba) was collected by filtration, washed with water (3 × 10 mL), and dried at 353 K overnight. To synthesize a proton-exchanged sample, 0.5 mL of concentrated HCl was dissolved in 14.5 mL of water. Then 0.3 g of as-synthesized material (Mo–Zn oxide or Mo–Mn oxide) was added. The mixture was stirred at 353 K for 6 h. The resulting solid was recovered by filtration, washed with water (3 × 10 mL), and dried at 353 K overnight.

*Elemental Analysis.* H–Mo–Zn oxide. Calcd for $Na_{0.6}Zn_3Mo_{12}O_{45}H_{22.3}$: Zn, 9.32; Mo, 54.73; Na, 0.66; H, 1.07. Found: Zn, 9.18; Mo, 54.98; Na, 0.67; H, 1.38.

Li–Mo–Zn oxide. Calcd for $Li_{0.7}Na_{0.8}Zn_3Mo_{12}O_{45}H_{21.4}$: Li, 0.23; Zn, 9.29; Mo, 54.51; Na, 0.87; H, 1.15. Found: Li, 0.07; Zn, 9.19; Mo, 54.88; Na, 0.72; H, 1.19.

$NH_4$–Mo–Zn oxide. Calcd for $Na_{0.1}N_{1.4}Zn_3Mo_{12}O_{45}H_{27}$: Na, 0.11; Zn, 9.27; Mo, 54.40; N, 0.93; H, 1.29. Found: Na, 0.08; Zn, 9.32; Mo, 54.37; N, 1.19; H, 1.45.

K–Mo–Zn oxide. Calcd for $K_{1.4}Na_{0.1}Zn_3Mo_{12}O_{45}H_{21.4}$: K, 2.55; Zn, 9.14; Mo, 53.65; Na, 0.11; H, 1.01. Found: K, 2.31; Zn, 9.26; Mo, 53.43; Na, 0.07; H, 1.16.

Rb–Mo–Zn oxide. Calcd for $Rb_{1.3}Na_{0.2}Zn_3Mo_{12}O_{45}H_{21.4}$: Rb, 5.04; Zn, 8.90; Mo, 52.22; Na, 0.21; H, 0.98. Found: Rb, 5.02; Zn, 8.93; Mo, 52.02; Na, 0.07; H, 1.10.

Cs–Mo–Zn oxide. Calcd for $Cs_{1.5}Zn_3Mo_{12}O_{45}H_{21.4}$: Cs, 8.71; Zn, 8.57; Mo, 50.31; Na, 0; H, 0.94. Found: Cs, 8.73; Zn, 8.67; Mo, 50.47; Na, 0; H, 1.01.

H–Mo–Mn oxide. Calcd for $N_{1.7}Mn_{2.2}Mo_{12}O_{43}H_{20.7}$: Mn, 6.03; Mo, 57.43; N, 1.19; H, 1.04. Found: Mn, 5.78; Mo, 57.75; N, 0.95; H, 1.47.

Li–Mo–Mn oxide. Calcd for $Li_{0.1}N_{2.0}Mn_{2.2}Mo_{12}O_{43}H_{21.5}$: Li, 0.03; Mn, 6.01; Mo, 57.26; N, 1.39; H, 1.08. Found: Li, 0.04; Mn, 6.12; Mo, 57.15; N, 1.28; H, 1.47.

Na–Mo–Mn oxide. Calcd for $Na_{0.4}N_{1.7}Mn_{2.2}Mo_{12}O_{43}H_{20.3}$: Na, 0.46; Mn, 6.00; Mo, 57.18; N, 1.18; H, 1.02. Found: Na, 0.52; Mn, 5.89; Mo, 56.99; N, 1.20; H, 1.38.

K–Mo–Mn oxide. Calcd for $K_{1.4}N_{0.7}Mn_{2.2}Mo_{12}O_{43}H_{16.3}$: K, 2.68; Mn, 5.92; Mo, 56.41; N, 0.48; H, 0.80. Found: K, 2.63; Mn, 6.37; Mo, 56.53; N, 0.38; H, 1.16.

Rb–Mo–Mn oxide. Calcd for $Rb_{1.5}N_{0.6}Mn_{2.2}Mo_{12}O_{43}H_{15.9}$: Rb, 6.07; Mn, 5.72; Mo, 54.49; N, 0.40; H, 0.76. Found: Rb, 6.03; Mn, 5.81; Mo, 54.55; N, 0.12; H, 1.07.

Cs–Mo–Mn oxide. Calcd for $Cs_{1.4}N_{0.7}Mn_{2.2}Mo_{12}O_{44}H_{18.3}$: Cs, 8.49; Mn, 5.52; Mo, 52.56; N, 0.45; H, 0.84. Found: Cs, 8.65; Mn, 5.44; Mo, 52.65; N, 0.17; H, 1.08.

Be–Mo–Zn oxide. Calcd for $Be_{0.3}Na_{0.9}Zn_3Mo_{12}O_{44}H_{19.4}$: Be, 0.13; Zn, 9.37; Mo, 54.97; Na, 0.99; H, 0.93. Found: Be, 0.12; Zn, 9.72; Mo, 54.72; Na, 1.04; H, 1.13.

Mg–Mo–Zn oxide. Calcd for $Mg_{0.6}Na_{0.3}Zn_3Mo_{12}O_{46}H_{23.4}$: Mg, 0.69; Zn, 9.22; Mo, 54.09; Na, 0.32; H, 1.11. Found: Mg, 0.62; Zn, 9.68; Mo, 53.77; Na, 0.44; H, 1.16.

Ca–Mo–Zn oxide. Calcd for $Ca_1Zn_3Mo_{12}O_{47}H_{24.9}$: Ca, 1.85; Zn, 9.06; Mo, 53.19; Na, 0; H, 1.16. Found: Ca, 1.75; Zn, 8.95; Mo, 52.79; Na, 0.03; H, 1.22.

Sr–Mo–Zn oxide. Calcd for $Sr_{0.8}Na_{0.1}Zn_3Mo_{12}O_{45}H_{21.2}$: Sr, 3.24; Zn, 9.08; Mo, 53.27; Na, 0.11; H, 0.98. Found: Sr, 3.29; Zn, 9.28; Mo, 52.94; Na, 0.13; H, 1.13.

Ba–Mo–Zn oxide. Calcd for $Ba_{1.4}Zn_3Mo_{12}O_{45}H_{20.1}$: Ba, 8.43; Zn, 8.60; Mo, 50.50; Na, 0; H, 0.89. Found: Ba, 8.30; Zn, 8.16; Mo, 50.34; Na, 0.02; H, 1.08.


dx.doi.org/10.1021/ic500630h | Inorg. Chem. 2014, 53, 7309–7318

Be−Mo−Mn oxide. Calcd for $Be_{0.2}N_{1.7}Mn_{2.2}Mo_{12}O_{45}H_{24.3}$: Be, 0.09; Mn, 5.92; Mo, 56.37; N, 1.17; H, 1.20. Found: Be, 0.07; Mn, 5.95; Mo, 56.01; N, 1.20; H, 1.36.

Mg−Mo−Mn oxide. Calcd for $Mg_{0.6}N_{1.2}Mn_{2.2}Mo_{12}O_{43}H_{18}$: Mg, 0.73; Mn, 6.01; Mo, 57.29; N, 0.84; H, 0.90. Found: Mg, 0.75; Mn, 6.10; Mo, 57.42; N, 0.86; H, 1.12.

Ca−Mo−Mn oxide. Calcd for $Ca_{0.9}N_1Mn_{2.2}Mo_{12}O_{45}H_{20.8}$: Ca, 1.75; Mn, 5.86; Mo, 55.80; N, 0.68; H, 1.02. Found: Ca, 1.78; Mn, 5.95; Mo, 55.60; N, 0.69; H, 1.28.

Sr−Mo−Mn oxide. Calcd for $Sr_{0.8}N_1Mn_{2.2}Mo_{12}O_{45}H_{21}$: Sr, 3.34; Mn, 5.76; Mo, 54.89; N, 0.67; H, 1.01. Found: Sr, 3.43; Mn, 5.55; Mo, 54.74; N, 0.67; H, 1.22.

Ba−Mo−Mn oxide. Calcd for $Ba_{1.6}Mn_{2.2}Mo_{12}O_{44}H_{14.4}$: Ba, 9.94; Mn, 5.47; Mo, 52.09; N, 0; H, 0.66. Found: Ba, 10.13; Mn, 5.24; Mo, 51.96; N, 0; H, 0.88.

**Characterization.** $N_2$ sorption isotherms were obtained by a BELSORP-max (BEL Japan Inc., Osaka, Japan) sorption analyzer at 77 K. The surface area was calculated by the Brunauer−Emmett−Teller (BET) method using an adsorption branch. Mo−V−Bi oxide was evacuated at 573 K for 2.5 h and the samples of Mo−Zn oxide and Mo−Mn oxide were evacuated at 473 K for 2.5 h before measurement. Powder XRD patterns were obtained on RINT2200 (Rigaku) with Cu K$\alpha$ radiation (tube voltage, 40 kV, tube current, 20 mA). Scanning electron microscopy (SEM) images were obtained with a HD-2000 microscope (Hitachi). Transmission electron microscopy (TEM) images were taken with a 200 kV transmission electron microscope (JEOL JEM-2010F). FT-IR analysis was carried out on a PARAGON 1000 analyzer (PerkinElmer). Raman spectra were recorded with a Renishaw inVia Raman microscope. Thermogravimetric−differential thermal analysis (TG-DTA) measurements were carried out up to 773 K at a heating rate of 10 K $min^{-1}$ under nitrogen (flow rate, 10 mL $min^{-1}$) and air (flow rate, 30 mL $min^{-1}$) flow with Thermo plus TG-8120 (Rigaku). Temperature-programmed desorption mass spectrometry (TPD-MS) measurements were carried out from 313 to 893 K at a heating rate of 10 K $min^{-1}$ under helium (flow rate, 50 mL $min^{-1}$). Samples were set up between two layers of quartz wool. A TPD apparatus (BEL Japan, Inc.) equipped with a quadrupole mass spectrometer (M-100QA; Anelva) was used to detect $NH_3$ ($m/z$ 16), $H_2O$ ($m/z$ 18), $O_2$ ($m/z$ 32), and $N_2$ ($m/z$ 28). For TPD-MS measurements of the materials after heat treatment, the samples were heated at 473 K under high vacuum for 2.5 h in a TPD instrument before measurements. X-ray photoelectron spectroscopy (XPS) was performed on a JPS-9010MC spectrometer (JEOL). The spectrometry energies were calibrated using the C 1s peak at 284.8 eV. Diffuse-reflectance (DR) UV−vis spectra were obtained using a JASCO V-570 spectrophotometer equipped with an ISN-470 reflectance spectroscopy accessory. Elemental compositions were determined by an inductive coupling plasma atomic emission spectroscopy (ICP-AES) method (ICPE-9000, Shimadzu). The CHN elemental composition was determined at Instrumental Analysis Division, Equipment Management Center, Creative Research Institution, Hokkaido University.

**Structure Determination and Computer-Based Simulation.** The structures of Mo−Zn and Mo−Mn oxides were determined by powder XRD. Powder XRD patterns were recorded on a RINT2200 diffractometer (Rigaku) with Cu K$\alpha$ radiation (tube voltage, 40 kV; tube current, 40 mA; scan speed, 1 deg $min^{-1}$; step, 0.01 deg). First, the powder XRD pattern was indexed by programs, including *DICVOL06*[30] and *X-cell*,[31] which gave the same results. After Pawley refinement was performed, the most reasonable space group was obtained. Then the Le Bail method[32] was applied for intensity extraction with the *EdPCR* program. The initial structure was solved by a charge-flipping algorithm.[33] The positions and types of heavy-metal atoms (Mo, Zn, and Mn) were obtained by analyzing the generated electron density maps. Most of the O atoms and cations were assigned according to the residual peaks, which were indicated by the charge-flipping algorithm, with consideration of the crystal structure of Mo−V−Bi oxide. The initial structures from the charge-flipping algorithm are shown in Supporting Information (SI) Tables S1 and S2.

The initial structures of Mo−Zn and Mo−Mn oxides were refined by powder XRD Rietveld refinement.[34] The lattice and pattern parameters of the material were first refined by Pawley refinement. Then isotropical temperature factors (see the SI for detailed information) were given for every atom in the initial structure. Rietveld analysis was started with the initial model of the material and lattice and pattern parameters from Pawley refinement. Every atom position was refined. The occupancy of atoms in the framework was fixed without further refinement, and occupancies of atoms in micropores were refined with consideration of the elemental analysis results. Finally, the pattern parameters were refined again for obtaining the lowest $R_{wp}$ value. Crystallographic and Rietveld analysis parameters are shown in SI Tables S3−S6.

Material modeling, the *X-cell* program, and Pawley and Rietveld refinement were performed with the *Materials Studio v6.1.0* package (Accelrys Software Inc.). *DICVOL06* and *EdPCR* were carried out with the *Fullprof* package. The charge-flipping algorithm was performed with *Superflip* in *Jana2006*, and electron density maps were generated with *Chimera 1.8.1*.

The Connolly surfaces and free space of POM-based materials were simulated by the *Atom Volume & Surfaces* program in *Materials Studio*. The diameters of the cage and channel were estimated from the Connolly surfaces of the cage and the channel with a Connolly radius of 1 Å,[35] and the shortest values are presented.

## RESULTS AND DISCUSSION

**Preparation of Mo−Zn and Mo−Mn Oxides.** Two novel POM-based crystalline metal oxides, Mo−Zn and Mo−Mn oxides, are synthesized under hydrothermal conditions. The hydrothermal reaction of $Na_2MoO_4{\cdot}2H_2O$, Mo metal, and $ZnCl_2$ at 448 K for 24 h produces Mo−Zn oxide, and the powder XRD profile of the solid is presented in Figure 2b. A profile similar to that of Mo−V−Bi oxide is observed. XRD peaks corresponding to $ZnMoO_4$, $MoO_2$, and unreacted Mo metal are also obtained in the crude solid.

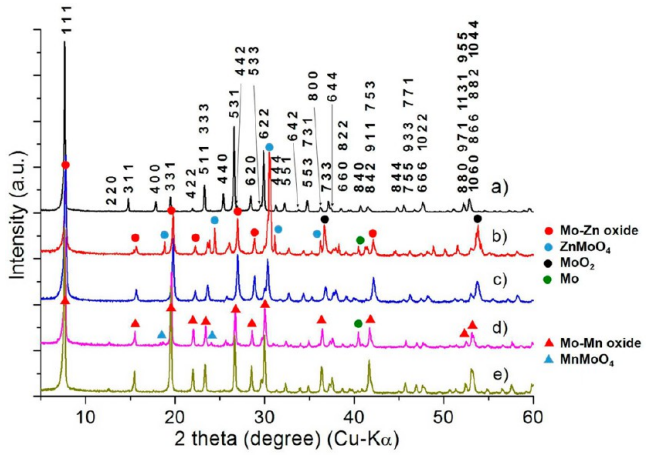


**Figure 2.** XRD patterns of (a) Mo−V−Bi oxide, (b) a crude solid of Mo−Zn oxide, (c) Mo−Zn oxide after purification, (d) a crude solid of Mo−Mn oxide, and (e) Mo−Mn oxide after purification. PDF number: $ZnMoO_4$, 00-025-1024; $MnMoO_4$, 01-082-2166; $MoO_2$, 00-050-0739; Mo, 00-004-0809.

The desired solid is isolatable by settlement of the obtained crude solid in water and decantation of the upper solution, because the desired Mo−Zn oxide is smaller than $ZnMoO_4$, $MoO_2$, and Mo metal (Figure 3 and SI Figure S1). The XRD profile of isolated Mo−Zn oxide is similar to that of Mo−V−Bi oxide (Figure 2c).


dx.doi.org/10.1021/ic500630h | Inorg. Chem. 2014, 53, 7309−7318

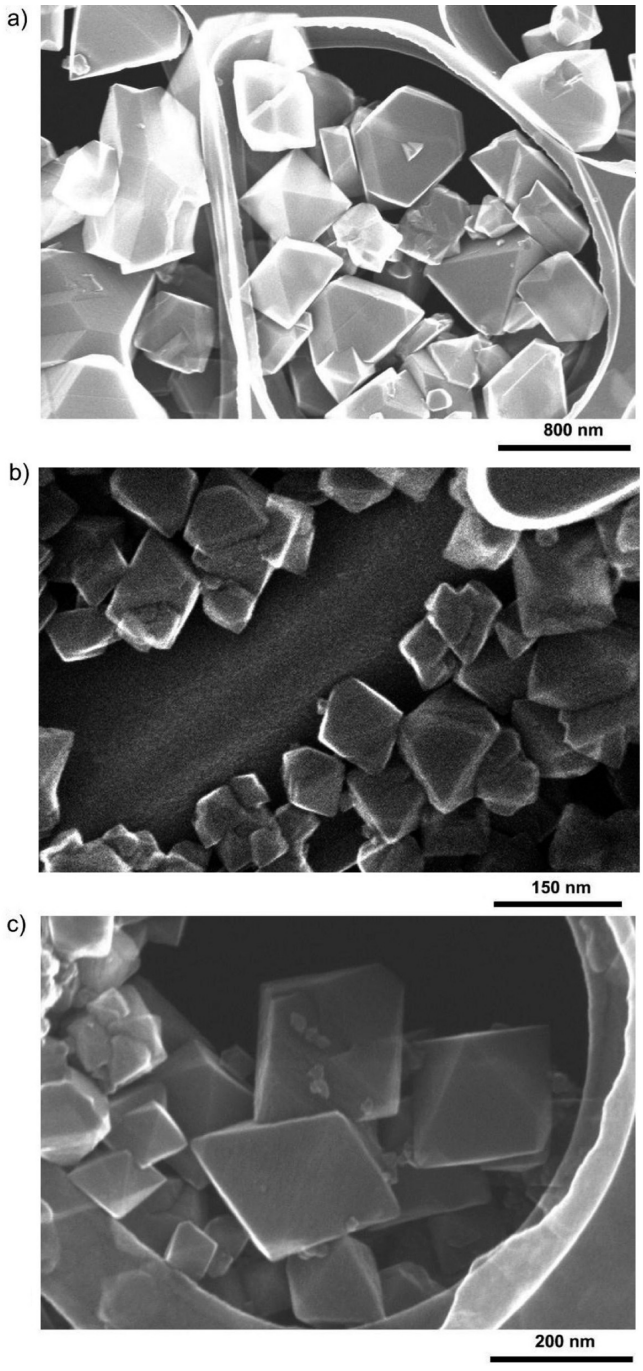


**Figure 3.** SEM images of (a) Mo−V−Bi, (b) Mo−Zn, and (c) Mo−Mn oxides.

Crystalline Mo−Mn oxide is prepared by the same method as that used for Mo−Zn oxide except for replacement of $ZnCl_2$ by MnO. A powder XRD profile similar to that of Mo−V−Bi oxide is observed in the profile of the resulting solid (Figure 2d). XRD peaks corresponding to $MnMoO_4$ and unreacted Mo metal are also detected.

The desired product is separated by settlement of the obtained crude solid in water and decantation of the upper solution, because the desired Mo−Mn oxide is smaller than $MnMoO_4$ and Mo metal (Figure 3 and Supporting Information Figure S1). The XRD profile of the isolated Mo−Mn oxide is also similar to that of Mo−V−Bi oxide (Figure 2e).

**Structural Characterizations of Mo−Zn and Mo−Mn Oxides.** The powder XRD profiles of Mo−Zn and Mo−Mn oxides are similar to that of Mo−V−Bi oxide with a slight shift of $2\theta$ and different intensity ratios (Figure 2 and SI Figure S2a), and XRD pattern indexing and Pawley refinement show that these three materials are cubic systems with the same space group of $Fd\bar{3}m$ and similar lattice parameters (Table 1). Mo−

**Table 1. Refined Parameters and Agreement Factors of Rietveld Analysis for Mo−Zn and Mo−Mn Oxides**

| | Mo−Zn oxide | Mo−Mn oxide |
|---|---|---|
| empirical formula | $O_{45.6}Na_{1.56}Zn_3Mo_{12}$ | $O_{47.9}Mn_{2.24}Mo_{12}$ |
| cryst syst | cubic | cubic |
| space group | $Fd\bar{3}m$ | $Fd\bar{3}m$ |
| $a = b = c$ (Å) | 19.4675 | 19.6578 |
| $\alpha = \beta = \gamma$ (deg) | 90 | 90 |
| $V$ (Å$^3$) | 7377.86 | 7596.34 |
| agreement factors | | |
| $R_{wp}$ (%) | 7.10 | 6.19 |
| $R_{wp}$(w/o bck) (%) | 12.09 | 11.92 |
| $R_p$ (%) | 5.35 | 4.66 |
| pattern parameter peak-shape function | pseudo-Voigt | pseudo-Voigt |
| fwhm | $U$ = 1.24597, $V$ = −0.65679, $W$ = 0.13636 | $U$ = 0.64154, $V$ = −0.26116, $W$ = 0.05624 |
| profile parameter line shift | $N_A$ = 1.02040, $N_B$ = −0.005 10 | $N_A$ = 1.03398, $N_B$ = −0.008 52 |
| instrument geometry | Bragg−Brentano | Bragg−Brentano |
| zero point | −1.01992 | −0.31358 |
| shift#1 | 0.93425 | 0.18755 |
| shift#2 | 0.09903 | 0.08589 |
| correction method | Berar−Baldinozzi | Berar−Baldinozzi |
| parameter | P1 = 0.19643, P2 = −0.10651, P3 = −0.48315, P4 = 0.20029 | P1 = 1.67562, P2 = 0.35040, P3 = −3.51892, P4 = −0.73820 |
| background coefficients | polynomial = 100 | polynomial = 100 |
| preferred orientation March−Dollase | R0 = 1.536 23 | R0 = 1.456 85 |

Zn and Mo−Mn oxides have octahedral morphologies that are similar to that of Mo−V−Bi oxide (Figure 3). Therefore, we consider the structures of Mo−Zn and Mo−Mn oxides to be similar to that of Mo−V−Bi oxide. The structure of Mo−V−Bi oxide has been determined by single-crystal X-ray analysis,[29] which showed that the material is comprised of $\varepsilon$-Keggin POM units, $\varepsilon$-$VMo_{9.4}V_{3.6}O_{40}$, with a $Bi^{III}$ linker (Figure 1). A V−O tetrahedron is surrounded by 12 M−O (M = Mo and V) octahedra to form the $\varepsilon$-Keggin-type POM, which is linked by $Bi^{III}$ to form a diamond-like framework. There are three metal sites in the framework of the materials: a central metal site, surrounding 12 metal sites, and linking metal sites in an asymmetric unit.

SEM images (Figure 3) of Mo−Zn and Mo−Mn oxides show that both of these materials are too small to perform single-crystal analysis (100−200 nm in one diameter). Therefore, structure analysis based on powder XRD is carried out.

For Mo−Zn oxide, the results obtained by using the charge-flipping algorithm reveal the three most intensive peaks of the electron density map with intensity order of surrounding metal sites > central metal site ∼ linking metal site (Figure 4a−c and


dx.doi.org/10.1021/ic500630h | Inorg. Chem. 2014, 53, 7309−7318

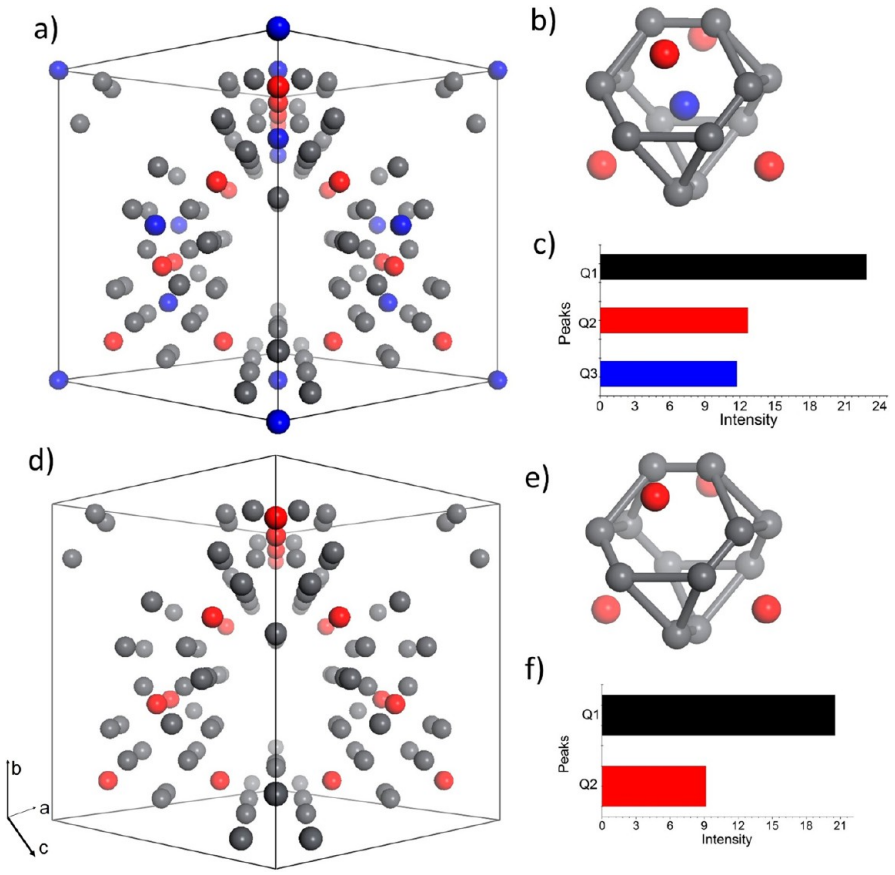


**Figure 4.** Schematic representations of the charge-flipping algorithm results: (a) electron density map from the charge-flipping method showing positions of the intensive peaks [surrounding metal sites (Q1; gray), linking metal sites (Q2; red), and central metal sites (Q3; blue)] in a unit cell; (b) $\varepsilon$-Keggin unit with four linking metal sites; (c) intensity difference of the peaks of Mo−Zn oxide; (d) electron density map from the charge-flipping method showing positions of the intensive peaks [surrounding metal sites (Q1; gray) and linking metal sites (Q2; red)] in a unit cell; (e) $\varepsilon$-Keggin unit with four linking metal sites; (f) intensity difference of the peaks of Mo−Mn oxide.

SI Table S1). Elemental analysis of Mo−Zn oxide reveals that the ratio of Mo:Zn is 12:3. These results indicate that Zn is present in the central and linking metal sites and that Mo is present in the surrounding metal sites. In the case of Mo−Mn oxide, the two most intensive peaks of the electron density map correspond to the surrounding metal sites and linking metal sites, where the intensity of the surrounding metal sites is much higher than that of the linking metal site (Figure 4d−f). A weak peak is found at the central metal site, indicating that the position is occupied partly or by light atoms (SI Table S2). Elemental analysis of Mo−Mn oxide reveals that the ratio of Mo:Mn is 12:2.2. These results indicate that Mo is present in the surrounding metal sites, Mn is present in the linking metal site, and the central metal site is occupied by Mn with 0.2 occupancy. Other sites are assigned as O atoms of the Keggin unit, countercations, and O atoms of water.

The initial structures of Mo−Zn and Mo−Mn oxides are refined with Rietveld refinement. Figure 5 shows the simulated powder XRD patterns of Mo−Zn and Mo−Mn oxides. The $R_{wp}$ values of Mo−Zn and Mo−Mn oxides are 7.10% and 6.19%, respectively. The results of Rietveld and elemental analyses demonstrate that the POM building blocks of Mo−Zn and Mo−Mn oxides are $\varepsilon$-Keggin POMs $\varepsilon$-$ZnMo_{12}O_{40}$ and $\varepsilon$-$Mn_{0.2}Mo_{12}O_{40}$, respectively (Figure 6a). A total of 12 $MoO_6$ octahedra surrounded an $MO_4$ (M = Zn or Mn) tetrahedron to form the $\varepsilon$-Keggin cores, which are connected by metal ions (Zn or Mn) in a tetrahedral fashion to form a 3D framework (Figure 6b). In the case of other $\varepsilon$-Keggin POMs, there are four capping metal ions for one $\varepsilon$-Keggin POM.[36−39] In the case of Mo−V−Bi, Mo−Zn, and Mo−Mn oxides, capping metal ions connect the POM units.

FT-IR and Raman spectra (SI Figure S3) of Mo−Zn and Mo−Mn oxides are similar to those of other $\varepsilon$-Keggin polyoxomolybdates, $[\varepsilon\text{-}H_2Mo_{12}O_{40}Ni_4(H_2O)]$[36] and $[\varepsilon\text{-}H_2Mo_{12}O_{40}Co_4(H_2O)]$.[40] $[\varepsilon\text{-}H_2Mo_{12}O_{40}Ni_4(H_2O)]$ and $[\varepsilon\text{-}H_2Mo_{12}O_{40}Co_4(H_2O)]$ are composed of $\varepsilon$-Keggin polyoxomolybdate $[\varepsilon\text{-}H_2Mo^{VI}{}_xMo^{V}{}_{12-x}O_{40}]$ and four $Ni^{2+}$ or $Co^{2+}$ on the hexagonal surfaces of the $\varepsilon$-Keggin polyoxomolybdate. These results confirm that the surrounding metal sites in the $\varepsilon$-Keggin cores are mostly occupied by Mo in Mo−Zn and Mo−Mn oxides.

High-resolution transmission electron microscopy (HRTEM) images are obtained to further confirm the structures. Figure 7 shows a comparison of the generated polyhedral image using the crystal structure of Mo−V−Bi oxide with HRTEM images of the materials along the (101) direction. HRTEM reveals characteristic face-centered-cubic lattice images for Mo−Zn and Mo−Mn oxides. The ordering of the rhombic black and white spots in the HRTEM images is exactly the same as the ordering of $\varepsilon$-Keggin POM building blocks and pores. The lattice parameters of the unit cells and distances of the (111) plane are also obtained from the HRTEM images, and they are in good agreement with the


dx.doi.org/10.1021/ic500630h | Inorg. Chem. 2014, 53, 7309−7318

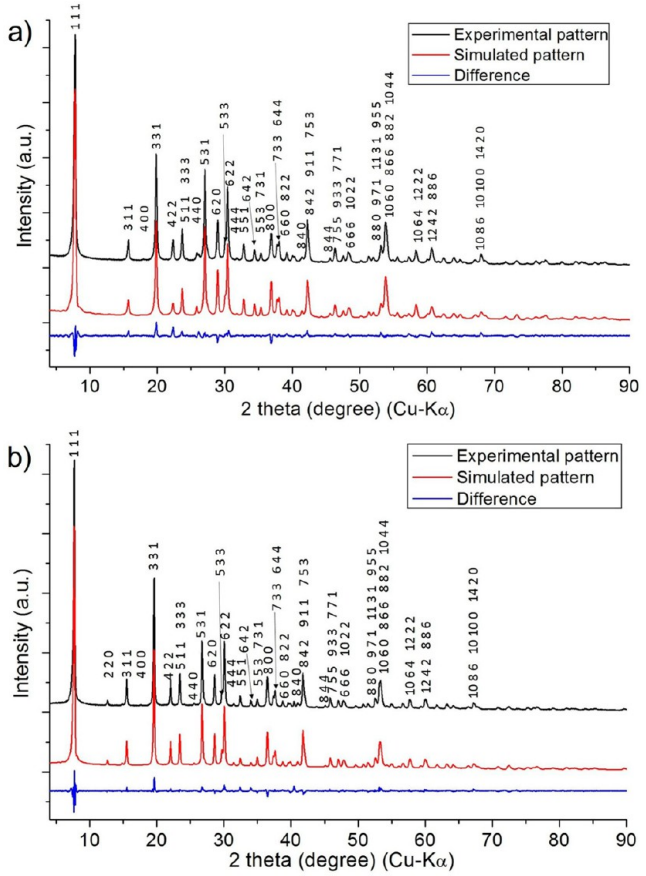


**Figure 5.** Comparison of the experimental XRD patterns with simulated XRD patterns using the Rietveld method: (a) Mo−Zn oxide, $R_{wp}$ = 7.10%; (b) Mo−Mn oxide, $R_{wp}$ = 6.19%.

results obtained from crystal structures of the materials (Figure 7d).

The oxidation states of the metal elements in Mo−Zn and Mo−Mn oxides are studied by XPS, and the results are presented in SI Figure S4. For linker metals, the bond valence sum (BVS) values of Zn and Mn are 2.13 and 1.93, respectively. For center metals, the BVS values of Zn and Mn are 2.14 and 2.24, respectively, confirming that the oxidation states of both $Zn^{II}$ and $Mn^{II}$ are 2+. The surrounding 12 Mo atoms are mostly reduced, as in the case of other $\varepsilon$-Keggin polyoxomolybdates.[7,36,38] In the case of Mo−Zn oxide, the ratio of $Mo^{VI}$:$Mo^{V}$ is 0.1:1.0. The ratio of $Mo^{VI}$:$Mo^{V}$ in Mo−Mn oxide is 1.0:1.0. The detailed chemical formulas of these two POM units are estimated to be $[\varepsilon\text{-}Zn^{II}Mo^{V}_{10.9}Mo^{VI}_{1.1}O_{40}\{Zn^{II}\}_2]^{12.9-}$ and $[\varepsilon\text{-}Mn^{II}_{0.2}Mo^{V}_{6}Mo^{VI}_{6}O_{40}\{Mn^{II}\}_2]^{9.6-}$.

The presence of water in Mo−Zn oxide and the presence of water and $NH_4^+$ in Mo−Mn oxide are confirmed by FT-IR analysis. The FT-IR spectrum (SI Figure S2b) of Mo−Mn oxide shows peak maxima at 1628 and 1401 $cm^{-1}$, corresponding to water and $NH_4^+$, respectively. For Mo−Zn oxide, a peak at 1630 $cm^{-1}$ corresponding to water is observed. The cationic species of Mo−Zn oxide is $Na^+$, which results from the starting agent of $Na_2MoO_4{\cdot}2H_2O$. The amounts of cationic species ($NH_4^+$ and $Na^+$) and water are estimated by elemental analysis. The detailed formulas of Mo−Zn and Mo−Mn oxides are $Na_{1.5}H_{11.4}[\varepsilon\text{-}Zn^{II}Mo^{V}_{10.9}Mo^{VI}_{1.1}O_{40}\{Zn^{II}\}_2]{\cdot}5H_2O$ and $(NH_4)_{2.1}H_{7.5}[\varepsilon\text{-}Mn^{II}_{0.2}Mo^{V}_{6}Mo^{VI}_{6}O_{40}\{Mn^{II}\}_2]{\cdot}4H_2O$, respectively.

Cages and channels exist in the materials. One cage is surrounded by 10 $\varepsilon$-Keggin POM units with metal-ion linkers ($Bi^{III}$, $Zn^{II}$, or $Mn^{II}$).[29] The cages are connected with channels in a tetrahedral fashion to form a periodical 3D pore system as FAU-type zeolites (Faujasite) do. The sizes of the cages are estimated from the Connolly surfaces (see details in the Experimental Section) to be 7.7, 7.6, and 7.6 Å and the sizes of the channels are estimated to be 3.4, 2.9, and 2.9 Å for Mo−V−Bi, Mo−Zn, and Mo−Mn oxides, respectively (Figure 6c). The pore systems of these materials are unique. In one direction, the tunnel of the pore is not straight but in a zigzag fashion (Figure 6d). The existing $NH_4^+$ (or $Na^+$) and water occupy the cages and channels in the as-synthesized materials.

TPD-MS analysis under helium flow shows that the water and $NH_4^+$ in the materials desorb with heat treatment (SI Figure S5). $m/z$ 16, 18, 28, and 32 are attributed to the signals of $NH_3$, water, $N_2$, and $O_2$, respectively. TPD-MS ($m/z$ 16) shows that Mo−V−Bi oxide has two $NH_4^+$ desorption processes when the temperature is increased to 873 K. One $NH_4^+$ has a weak interaction with the framework and desorbs at 433 K, and the other has a strong interaction with the framework and desorbs at 633 K.[29] Mo−Mn oxide only shows a peak at 593 K in the TPD profile ($m/z$ 16), indicating only one kind of $NH_4^+$ in the framework. Mo−Zn oxide does not have any $NH_4^+$ in the structure, and therefore no signal of $m/z$ 16 is found in the TPD profile. For water desorption, TPD profiles of these three materials show two water desorption processes. TG-DTA of Mo−Zn and Mo−Mn oxides under nitrogen flow (SI Figure S5d,e) shows weight losses of 8.2% and 7.2% until ca. 620 K for Mo−Zn and Mo−Mn oxides, respectively. The theoretical weight loss related to removal of the included water calculated from the chemical formula is 4.2% for Mo−Zn oxide, and that related to removal of the included water and ammonium cation is 5.4% for Mo−Mn oxide, which are remarkably smaller than the observed weight losses of the oxides. It is known that heating of POMs generates water from protons and O atoms of POM.[41,42] The calculated weight losses of removal of the included water, ammonium cation, and water generated from protons and O atoms of polyoxomolybdate are 8.7% and 8.7% for Mo−Zn and Mo−Mn oxides, respectively, which are close to the observed values. Therefore, we conclude that heating Mo−Zn and Mo−Mn oxides generates water from protons and O atoms of polyoxomolybdates.

**Thermal Stability.** Mo−V−Bi oxide is stable, and the structure of the framework is maintained under the condition of heat treatment at 623 K under a nitrogen gas atmosphere. The stabilities of these two materials are tested by calcination at different temperatures under nitrogen gas. The materials are stable up to 523 K. The powder XRD patterns (SI Figure S6) of the samples calcined at 573 K show that the peak intensities decreased remarkably and FT-IR spectra of the materials also change (SI Figure S7), indicating that both Mo−Zn and Mo−Mn oxides start to collapse at 573 K and are less stable than Mo−V−Bi oxide.

The guest molecules, ammonia and water, in the as-synthesized POM-based materials can be removed by sufficient heat treatment without structural decomposition. Mo−V−Bi oxide is calcined at 623 K for 2 h under a nitrogen atmosphere followed by treatment at 573 K for 2.5 h under high vacuum. Mo−Zn and Mo−Mn oxides are treated at 473 K for 2.5 h under high vacuum. Most of the guest molecules occupying the cages and channels are removed by heat treatment (SI Figure S8) without collapse of the structures (SI Figure S6). TPD-MS


dx.doi.org/10.1021/ic500630h | Inorg. Chem. 2014, 53, 7309−7318

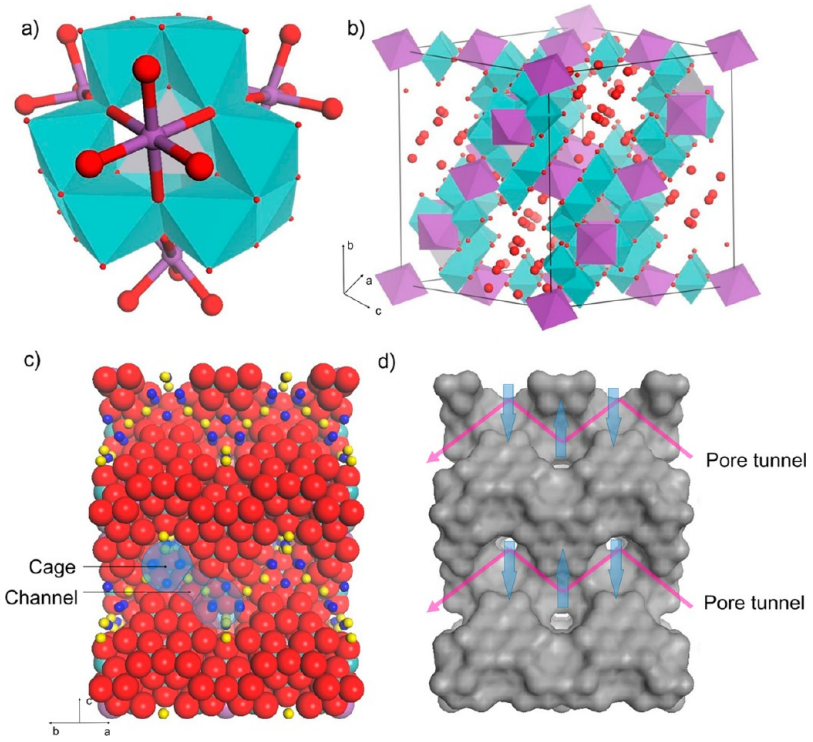


**Figure 6.** Polyhedral representations of (a) $\varepsilon$-Keggin POM with capping metal ions. (b) Unit cell. Surrounding $MoO_6$ octahedra: blue. Central $MO_4$ tetrahedra: gray. Metal-ion linkers (Bi, Zn, and Mn): purple. Oxygen: red. (c) CPK (Corey, Pauling, and Koltun) representations of the (110) plane. Framework oxygen: red. Species in the channel: yellow. Species in the cages: deep blue. (d) Connolly surface of the materials in the (110) plane. The pink arrow shows the pore tunnel along the (110) plane, and the blue arrow shows the pore tunnel perpendicular to the (110) plane.

($m/z$ 16 and 18) profiles of the samples treated at 473 K for 2.5 h under high vacuum show that small amounts of strongly bound water and ammonia remained.

$N_2$ adsorption−desorption measurement of calcined Mo−V−Bi oxide at 623 K shows a characteristic type I isotherm (Figure 8), indicating that the material is a microporous material. Mo−Zn and Mo−Mn oxides are heated at 473 K for 2.5 h under high vacuum, which are expected to remove most of $NH_3$ and water, before sorption measurement (SI Figure S8). The results show that the micropores of Mo−Zn and Mo−Mn oxides are also opened, although the adsorbed volume of $N_2$ on the materials is lower than that on Mo−V−Bi oxide. Surface areas are calculated as 60, 37, and 27 $m^2\ g^{-1}$ for Mo−V−Bi, Mo−Zn, and Mo−Mn oxides, respectively, using the BET method. The largest BET surface area mainly results from the highly opened micropores of Mo−V−Bi oxide. The less opened micropores of Mo−Zn and Mo−Mn oxides might be caused by the remaining $NH_4^+$ and $Na^+$, which would block pores and decrease the pore volume of the materials.[29]

**Ion-Exchange Property.** POM-based materials that show ion-exchange property are interesting.[43,44] Mo−V−Bi oxide shows an ion-exchange property similar to that of zeolite.[29] There are two kinds of $NH_4^+$ in Mo−V−Bi oxide, a strongly bound one and a weakly bound one. Small cations, including $H^+$, $Li^+$, and $Na^+$, selectively replace the weakly bound $NH_4^+$, and large cations, including $K^+$, $Rb^+$, and $Cs^+$, selectively replace the strongly bound one. We confirm that $K^+$ is present in the channel and that strongly bound $NH_4^+$ exists in the channel. Mo−Zn and Mo−Mn oxides show ion-exchange properties. The countercations, $NH_4^+$ in Mo−Mn oxide and $Na^+$ in Mo−Zn oxide, are exchangeable with other cations. Various countercations, including $H^+$, $Li^+$, $Na^+$, $K^+$, $Rb^+$, and $Cs^+$, were tested for ion exchange with Mo−Zn and Mo−Mn oxides. After the ion-exchange process, the ion-exchanged samples are characterized by powder XRD (SI Figure S9), which shows that all of the characteristic peaks of Mo−Zn and Mo−Mn oxides are retained in the corresponding ion-exchanged materials and demonstrate that the basic structures of the materials are unchanged. For $K^+$-, $Rb^+$-, and $Cs^+$-exchanged samples, powder XRD patterns reveal that the relative peak intensity of ion-exchanged samples changes compared with that of the as-synthesized sample. Moreover, diffraction peaks shift, especially after ion exchange with $Rb^+$ and $Cs^+$, which implies a slight alteration of the lattice parameters (SI Figure S9). In FT-IR spectra of the materials, the vibration peaks of the POM moiety are unchanged, indicating the high stability of the materials during the ion-exchange process. A decrease of the $NH_4^+$ peaks in FT-IR spectra of Mo−Mn oxide also indicates that $NH_4^+$ is replaced by other countercations (SI Figure S10).

Elemental analysis confirms that the cations are exchanged with $NH_4^+$ or $Na^+$ and introduced into the materials. The chemical formulas of the ion-exchanged samples are summarized in Table 2. The results show that the ion-exchange properties of the materials depend on the size of the ions. Large cations, including $K^+$, $Rb^+$, and $Cs^+$, show a high ion-exchange capacity for both Mo−Zn and Mo−Mn oxides. Small ions, $H^+$, $Li^+$, and $Na^+$, are not as efficient as the large ions to replace $NH_4^+$ or $Na^+$ in as-synthesized materials of Mo−Zn and Mo−Mn oxides. Elemental analysis further shows that the amounts of Mo, Zn, and Mn remain constant after the ion-exchange process, indicating that Mo, Zn, and Mn are in the frameworks of the materials.

Furthermore, the ion-exchange properties of Mo−Zn and Mo−Mn oxides with alkaline-earth metal ions are also


dx.doi.org/10.1021/ic500630h | Inorg. Chem. 2014, 53, 7309−7318

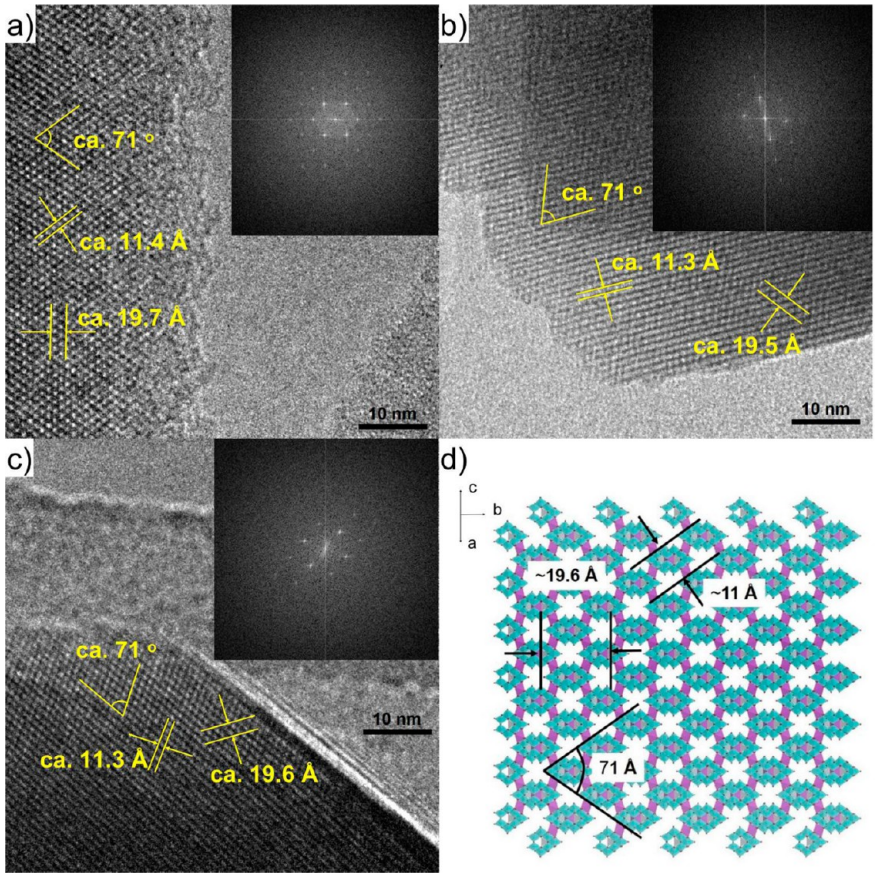


**Figure 7.** HRTEM images of (a) Mo−V−Bi, (b) Mo−Zn, and (c) Mo−Mn oxides with comparison of (d) the polyhedral representation. Inset: power spectra.

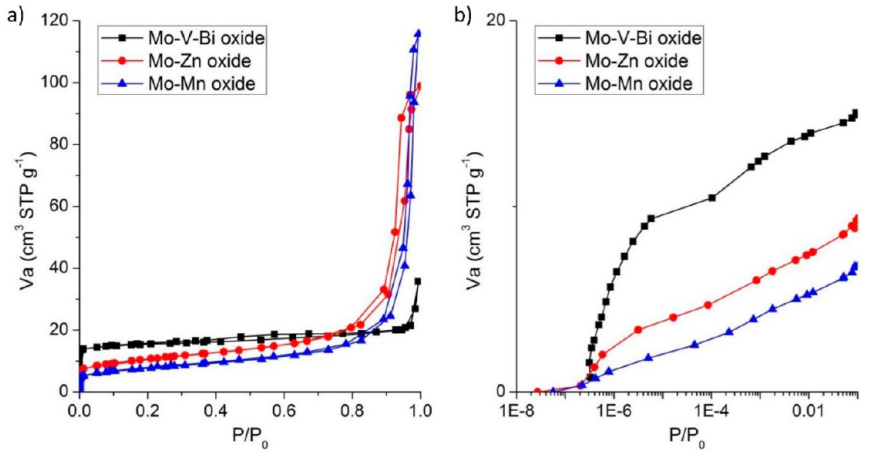


**Figure 8.** (a) $N_2$ adsorption−desorption isotherms of Mo−V−Bi, Mo−Zn, and Mo−Mn oxides and (b) the low pressure range.

investigated. After ion exchange, the basic structures of the materials do not change, as indicated by powder XRD patterns (SI Figure S11) and FT-IR spectra (SI Figure S12). Elemental analysis shows that the alkaline-earth metal ions are successfully replaced by the original cations in the materials. Chemical formulas calculated from elemental analysis show that heavy alkaline-earth metal ions, such as $Ba^{2+}$ and $Sr^{2+}$, can exchange not only with cation species ($Na^+$ or $NH_4^+$) but also with protons in the materials (Table 3).

**Redox Behavior.** A comparison of TG-DTA of Mo−Zn and Mo−Mn oxides under nitrogen and air flow (SI Figure S5) shows that weight losses in air flow are less than those in nitrogen flow. These results indicate that Mo−Zn and Mo−Mn oxides are oxidized by air. After heating of these oxides in air at 398 K for 2 h, all characteristic peaks of the XRD patterns (SI Figure S13) are retained with a peak shift to higher angles. These results indicate that the structures of these oxides are stable under the heating conditions and the lattice parameters become smaller. Oxidation of $Mo^V$ to $Mo^{VI}$ is confirmed by XPS (Table 4 and SI Figure S14 and Table S7).

Furthermore, reduction of the materials is conducted under hydrogen flow at 423 K. After reduction, the basic structures of


dx.doi.org/10.1021/ic500630h | Inorg. Chem. 2014, 53, 7309−7318

**Table 2. Chemical Formulas of Mo−Zn and Mo−Mn Oxides with Alkaline-Metal Ions**

| | formula |
|---|---|
| as-synthesized Mo−Zn oxide | $Na_{1.5}H_{11.4}[\varepsilon\text{-}ZnMo_{12}O_{40}\{Zn\}_2]\cdot 5H_2O$ |
| H−Mo−Zn oxide | $Na_{0.6}H_{12.3}[\varepsilon\text{-}ZnMo_{12}O_{40}\{Zn\}_2]\cdot 5H_2O$ |
| Li−Mo−Zn oxide | $Li_{0.7}Na_{0.8}H_{11.4}[\varepsilon\text{-}ZnMo_{12}O_{40}\{Zn\}_2]\cdot 5H_2O$ |
| $NH_4$−Mo−Zn oxide | $(NH_4)_{1.4}Na_{0.1}H_{11.4}[\varepsilon\text{-}ZnMo_{12}O_{40}\{Zn\}_2]\cdot 5H_2O$ |
| K−Mo−Zn oxide | $K_{1.4}Na_{0.1}H_{11.4}[\varepsilon\text{-}ZnMo_{12}O_{40}\{Zn\}_2]\cdot 5H_2O$ |
| Rb−Mo−Zn oxide | $Rb_{1.3}Na_{0.2}H_{11.4}[\varepsilon\text{-}ZnMo_{12}O_{40}\{Zn\}_2]\cdot 5H_2O$ |
| Cs−Mo−Zn oxide | $Cs_{1.5}H_{11.4}[\varepsilon\text{-}ZnMo_{12}O_{40}\{Zn\}_2]\cdot 5H_2O$ |
| as-synthesized Mo−Mn oxide | $(NH_4)_{2.1}H_{7.5}[\varepsilon\text{-}Mn_{0.2}Mo_{12}O_{40}\{Mn\}_2]\cdot 4H_2O$ |
| H−Mo−Mn oxide | $(NH_4)_{1.7}H_{7.9}[\varepsilon\text{-}Mn_{0.2}Mo_{12}O_{40}\{Mn\}_2]\cdot 3H_2O$ |
| Li−Mo−Mn oxide | $Li_{0.1}(NH_4)_{2.0}H_{7.5}[\varepsilon\text{-}Mn_{0.2}Mo_{12}O_{40}\{Mn\}_2]\cdot 3H_2O$ |
| Na−Mo−Mn oxide | $Na_{0.4}(NH_4)_{1.7}H_{7.5}[\varepsilon\text{-}Mn_{0.2}Mo_{12}O_{40}\{Mn\}_2]\cdot 3H_2O$ |
| K−Mo−Mn oxide | $K_{1.4}(NH_4)_{0.7}H_{7.5}[\varepsilon\text{-}Mn_{0.2}Mo_{12}O_{40}\{Mn\}_2]\cdot 3H_2O$ |
| Rb−Mo−Mn oxide | $Rb_{1.5}(NH_4)_{0.6}H_{7.5}[\varepsilon\text{-}Mn_{0.2}Mo_{12}O_{40}\{Mn\}_2]\cdot 3H_2O$ |
| Cs−Mo−Mn oxide | $Cs_{1.4}(NH_4)_{0.7}H_{7.5}[\varepsilon\text{-}Mn_{0.2}Mo_{12}O_{40}\{Mn\}_2]\cdot 4H_2O$ |

**Table 3. Chemical Formulas of Mo−Zn and Mo−Mn Oxides with Alkaline-Earth Metal Ions**

| | formula |
|---|---|
| as-synthesized Mo−Zn oxide | $Na_{1.5}H_{11.4}[\varepsilon\text{-}ZnMo_{12}O_{40}\{Zn\}_2]\cdot 5H_2O$ |
| Be−Mo−Zn oxide | $Be_{0.3}Na_{0.9}H_{11.4}[\varepsilon\text{-}ZnMo_{12}O_{40}\{Zn\}_2]\cdot 4H_2O$ |
| Mg−Mo−Zn oxide | $Mg_{0.6}Na_{0.3}H_{11.4}[\varepsilon\text{-}ZnMo_{12}O_{40}\{Zn\}_2]\cdot 6H_2O$ |
| Ca−Mo−Zn oxide | $CaH_{10.9}[\varepsilon\text{-}ZnMo_{12}O_{40}\{Zn\}_2]\cdot 7H_2O$ |
| Sr−Mo−Zn oxide | $Sr_{0.8}Na_{0.1}H_{11.2}[\varepsilon\text{-}ZnMo_{12}O_{40}\{Zn\}_2]\cdot 5H_2O$ |
| Ba−Mo−Zn oxide | $Ba_{1.4}H_{10.1}[\varepsilon\text{-}ZnMo_{12}O_{40}\{Zn\}_2]\cdot 5H_2O$ |
| as-synthesized Mo−Mn oxide | $(NH_4)_{2.1}H_{7.5}[\varepsilon\text{-}Mn_{0.2}Mo_{12}O_{40}\{Mn\}_2]\cdot 4H_2O$ |
| Be−Mo−Mn oxide | $Be_{0.2}(NH_4)_{1.7}H_{7.5}[\varepsilon\text{-}Mn_{0.2}Mo_{12}O_{40}\{Mn\}_2]\cdot 5H_2O$ |
| Mg−Mo−Mn oxide | $Mg_{0.6}(NH_4)_{1.2}H_{7.2}[\varepsilon\text{-}Mn_{0.2}Mo_{12}O_{40}\{Mn\}_2]\cdot 3H_2O$ |
| Ca−Mo−Mn oxide | $Ca_{0.9}(NH_4)_1H_{6.8}[\varepsilon\text{-}Mn_{0.2}Mo_{12}O_{40}\{Mn\}_2]\cdot 5H_2O$ |
| Sr−Mo−Mn oxide | $Sr_{0.8}(NH_4)_1H_7[\varepsilon\text{-}Mn_{0.2}Mo_{12}O_{40}\{Mn\}_2]\cdot 5H_2O$ |
| Ba−Mo−Mn oxide | $Ba_{1.6}H_{6.4}[\varepsilon\text{-}Mn_{0.2}Mo_{12}O_{40}\{Mn\}_2]\cdot 4H_2O$ |

**Table 4. Ratio of Mo Ions with Different Oxidation States in Mo−Zn and Mo−Mn Oxides after Redox Treatment and Their Corresponding Chemical Formulas**

| | ratio of Mo ions | chemical formula |
|---|---|---|
| Mo−Zn oxide | $Mo^{VI}:Mo^{V}$ = 0.10 | $Na_{1.5}H_{11.4}[\varepsilon\text{-}Zn^{II}Mo^{V}_{10.9}Mo^{VI}_{1.1}O_{40}\{Zn^{II}\}_2]$ |
| Mo−Zn oxide heated at 398 K in air | $Mo^{VI}:Mo^{V}$ = 0.85 | $Na_{1.5}H_7[\varepsilon\text{-}Zn^{II}Mo^{V}_{6.5}Mo^{VI}_{5.5}O_{40}\{Zn^{II}\}_2]$ |
| Mo−Zn oxide heated at 423 K under hydrogen flow | $Mo^{V}:Mo^{IV}$ = 0.25 | $Na_{1.5}H_{22.1}[\varepsilon\text{-}Zn^{II}Mo^{V}_{2.4}Mo^{IV}_{9.6}O_{40}\{Zn^{II}\}_2]$ |
| Mo−Mn oxide | $Mo^{VI}:Mo^{V}$ = 1.00 | $(NH_4)_{2.1}H_{7.5}[\varepsilon\text{-}Mn^{II}_{0.2}Mo^{V}_{6}Mo^{VI}_{6}O_{40}\{Mn^{II}\}_2]$ |
| Mo−Mn oxide heated at 398 K in air | $Mo^{VI}:Mo^{V}$ = 6.10 | $(NH_4)_{2.1}H_{3.2}[\varepsilon\text{-}Mn^{II}_{0.2}Mo^{V}_{1.7}Mo^{VI}_{10.3}O_{40}\{Mn^{II}\}_2]$ |
| Mo−Mn oxide heated at 423 K under hydrogen flow | $Mo^{VI}:Mo^{V}$ = 1.00 | $(NH_4)_{2.1}H_{7.5}[\varepsilon\text{-}Mn^{II}_{0.2}Mo^{V}_{6}Mo^{VI}_{6}O_{40}\{Mn^{II}\}_2]$ |

the materials do not change (SI Figure S13). XPS results (Table 4 and SI Figure S14 and and Table S7) demonstrate that the Mo ion in Mo−Zn oxide can be reduced to $Mo^{V}$ and $Mo^{IV}$, while the Mo ion is not reduced in Mo−Mn oxide under the current conditions. Furthermore, redox treatments of the materials affect the DR UV−vis spectra of the materials (SI Figure S15).

These results indicate that these oxides can accept and release electrons without collapse of the structures. Further investigations to understand and control the redox behavior of these materials are now in progress in our group.

## CONCLUSION

Two new $\varepsilon$-Keggin polyoxomolybdate-based 3D framework materials, cubic Mo−Zn and Mo−Mn oxides, have been successfully synthesized and characterized. In both oxides, $\varepsilon$-Keggin polyoxomolybdates with 12 Mo atoms, $[\varepsilon\text{-}ZnMo_{12}O_{40}]$ or $[\varepsilon\text{-}Mn_{0.2}Mo_{12}O_{40}]$, are linked by $Zn^{II}$ or $Mn^{II}$ ions to form 3D diamond-like frameworks. The guest molecules in as-synthesized materials can be mostly removed by heat treatment (473 K), although they are thermally less stable than the previously reported Mo−V−Bi oxide. These oxides show ion-exchange properties similar to those of zeolite materials. Furthermore, these oxides can accept and release electrons without collapse of the structures. Our results, indicating that a variety of transition metals can be incorporated into the $\varepsilon$-Keggin polyoxomolybdate-based materials, open a door for the development of $\varepsilon$-Keggin polyoxomolybdate-based 3D framework materials as functional materials, such as ion-exchange, catalyst, adsorption, and magnetic materials.

## ASSOCIATED CONTENT

### Supporting Information

Detailed experimental procedures, including figures and tables. This material is available free of charge via the Internet at http://pubs.acs.org.

## AUTHOR INFORMATION


### Corresponding Authors

*E-mail: sadakane09@hiroshima-u.ac.jp. Phone: +81-82-424-4456. Fax: +81-82-424-5494.

*E-mail: ueda@cat.hokudai.ac.jp. Phone: +81-11-706-9164. Fax: +81-11-706-9163.


### Author Contributions

All authors have given approval to the final version of the manuscript.

### Notes

The authors declare no competing financial interest.

## ACKNOWLEDGMENTS

This work was financially supported by a Grant-in-Aid for Scientific Research (A) (Grant 2324-6135) from the Ministry of Education, Culture, Sports, Science, and Technology, Japan. M.S. thanks PRESTO, JST, for financial support.

## REFERENCES


(1) Special thematic issue on polyoxometalates: Hill, C. L. *Chem. Rev.* **1998**, *98*, 1−390.

(2) Special thematic issue on polyoxometalates: Cronin, L.; Müller, A. *Chem. Soc. Rev.* **2012**, *41*, 7325−7648.

(3) Pope, M. T. *Heteropoly and Isopoly Oxometalates*; Springer-Verlag: Berlin, 1983.

(4) Dolbecq, A.; Mialane, P.; Secheresse, F.; Keita, B.; Nadjo, L. *Chem. Commun.* **2012**, *48*, 8299−8316.

(5) Mandic, S.; Healey, M. R.; Gotthardt, J. M.; Alley, K. G.; Gable, R. W.; Ritchie, C.; Boskovic, C. *Eur. J. Inorg. Chem.* **2013**, 1631−1634.
(6) Nohra, B.; El Moll, H.; Rodriguez Albelo, L. M.; Mialane, P.; Marrot, J.; Mellot-Draznieks, C.; O'Keeffe, M.; Biboum, R. N.; Lemaire, J.; Keita, B.; Nadjo, L.; Dolbecq, A. *J. Am. Chem. Soc.* **2011**, *133*, 13363−13374.
(7) Rodriguez-Albelo, L. M.; Rabdel Ruiz-Salvador, A.; Sampieri, A.; Lewis, D. W.; Gomez, A.; Nohra, B.; Mialane, P.; Marrot, J.; Secheresse, F.; Mellot-Draznieks, C.; Biboum, R. N.; Keita, B.; Nadjo, L.; Dolbecq, A. *J. Am. Chem. Soc.* **2009**, *131*, 16078−16087.
(8) Song, J.; Luo, Z.; Britt, D. K.; Furukawa, H.; Yaghi, O. M.; Hardcastle, K. I.; Hill, C. L. *J. Am. Chem. Soc.* **2011**, *133*, 16839−16846.
(9) Sun, C.-Y.; Liu, S.-X.; Liang, D.-D.; Shao, K.-Z.; Ren, Y.-H.; Su, Z.-M. *J. Am. Chem. Soc.* **2009**, *131*, 1883−1888.
(10) Kamiya, Y.; Sadakane, M.; Ueda, W. Heteropoly Compounds. In *Comprehensive Inorganic Chemistry II*; Reedijk, J., Poeppelmeier, K., Eds.; Elsevier: Oxford, U.K., 2013; Vol. 7, pp 185−204.
(11) Eguchi, R.; Uchida, S.; Mizuno, N. *J. Phys. Chem. C* **2012**, *116*, 16105−16110.
(12) Eguchi, R.; Uchida, S.; Mizuno, N. *Angew. Chem., Int. Ed.* **2012**, *51*, 1635−1639.
(13) Jiang, C.; Lesbani, A.; Kawamoto, R.; Uchida, S.; Mizuno, N. *J. Am. Chem. Soc.* **2006**, *128*, 14240−14241.
(14) Kawamoto, R.; Uchida, S.; Mizuno, N. *J. Am. Chem. Soc.* **2005**, *127*, 10560−10567.
(15) Uchida, S.; Eguchi, R.; Nakamura, S.; Ogasawara, Y.; Kurosawa, N.; Mizuno, N. *Chem. Mater.* **2012**, *24*, 325−330.
(16) Uchida, S.; Lesbani, A.; Ogasawara, Y.; Mizuno, N. *Inorg. Chem.* **2012**, *51*, 775−777.
(17) Uchida, S.; Mizuno, N. *Coord. Chem. Rev.* **2007**, *251*, 2537−2546.
(18) Uchida, S.; Hikichi, S.; Akatsuka, T.; Tanaka, T.; Kawamoto, R.; Lesbani, A.; Nakagawa, Y.; Uehara, K.; Mizuno, N. *Chem. Mater.* **2007**, *19*, 4694−4701.
(19) Sadakane, M.; Endo, K.; Kodato, K.; Ishikawa, S.; Murayama, T.; Ueda, W. *Eur. J. Inorg. Chem.* **2013**, 1731−1736.
(20) Sadakane, M.; Watanabe, N.; Katou, T.; Nodasaka, Y.; Ueda, W. *Angew. Chem., Int. Ed.* **2007**, *46*, 1493−1496.
(21) Sadakane, M.; Yamagata, K.; Kodato, K.; Endo, K.; Toriumi, K.; Ozawa, Y.; Ozeki, T.; Nagai, T.; Matsui, Y.; Sakaguchi, N.; Pyrz, W. D.; Buttrey, D. J.; Blom, D. A.; Vogt, T.; Ueda, W. *Angew. Chem., Int. Ed.* **2009**, *48*, 3782−3786.
(22) Sadakane, M.; Ohmura, S.; Kodato, K.; Fujisawa, T.; Kato, K.; Shimidzu, K.; Murayama, T.; Ueda, W. *Chem. Commun.* **2011**, *47*, 10812−10814.
(23) Sadakane, M.; Kodato, K.; Kuranishi, T.; Nodasaka, Y.; Sugawara, K.; Sakaguchi, N.; Nagai, T.; Matsui, Y.; Ueda, W. *Angew. Chem., Int. Ed.* **2008**, *47*, 2493−2496.
(24) Wang, F.; Ueda, W. *Top. Catal.* **2008**, *50*, 90−97.
(25) Wang, F.; Ueda, W. *Catal. Today* **2009**, *144*, 358−361.
(26) Konya, T.; Katou, T.; Murayama, T.; Ishikawa, S.; Sadakane, M.; Buttrey, D.; Ueda, W. *Catal. Sci. Technol.* **2013**, *3*, 380−387.
(27) Watanabe, N.; Ueda, W. *Ind. Eng. Chem. Res.* **2006**, *45*, 607−614.
(28) Mitchell, S. G.; Streb, C.; Miras, H. N.; Boyd, T.; Long, D.-L.; Cronin, L. *Nat. Chem.* **2010**, *2*, 308−312.
(29) Zhang, Z.; Sadakane, M.; Murayama, T.; Izumi, S.; Yasuda, N.; Sakaguchi, N.; Ueda, W. *Inorg. Chem.* **2014**, *53*, 903−911.
(30) Boultif, A.; Louer, D. *J. Appl. Crystallogr.* **2004**, *37*, 724−731.
(31) Neumann, M. A. *J. Appl. Crystallogr.* **2003**, *36*, 356−365.
(32) Le Bail, A. *Powder Diffr.* **2008**, *23*, S5−S12.
(33) Palatinus, L.; Chapuis, G. *J. Appl. Crystallogr.* **2007**, *40*, 786−790.
(34) Young, R. A. *The Rietveld Method*; Young, R. A., Ed.; Oxford University Press: Oxford, U.K., 1995.
(35) Kim, D.-S.; Ryu, J.; Park, R. *J. Comput. Sci. Technol.* **2006**, *21*, 255−260.
(36) Müller, A.; Beugholt, C.; Kogerler, P.; Bogge, H.; Bud'ko, S.; Luban, M. *Inorg. Chem.* **2000**, *39*, 5176−5177.
(37) Sloboda-Rozner, D.; Neimann, K.; Neumann, R. *J. Mol. Catal. A: Chem.* **2007**, *262*, 109−113.
(38) Mialane, P.; Dolbecq, A.; Lisnard, L.; Mallard, A.; Marrot, J.; Secheresse, F. *Angew. Chem., Int. Ed.* **2002**, *41*, 2398−2401.
(39) Tucher, J.; Nye, L. C.; Ivanovic-Burmazovic, I.; Notarnicola, A.; Streb, C. *Chem.—Eur. J.* **2012**, *18*, 10949−10953.
(40) Ellern, A.; Kögerler, P. *Acta Crystallogr., Sect. C* **2012**, *68*, i17−i19.
(41) Tong, X.; Zhu, W.; Wu, Q.; Qian, X.; Liu, Z.; Yan, W.; Gong, J. *J. Alloys Compd.* **2011**, *509*, 7768−7772.
(42) Wu, Q.; Wang, S.; Li, D.; Xie, X. *Inorg. Chem. Commun.* **2002**, *5*, 308−311.
(43) Rehder, D.; Haupt, E. T. K.; Bögge, H.; Müller, A. *Chem.—Asian J.* **2006**, *1*, 76−81.
(44) Rehder, D.; Haupt, E. T. K.; Müller, A. *Magn. Reson. Chem.* **2008**, *46*, S24−S29.